



# Neutron–proton bremsstrahlung as a possible probe of high-momentum component in nucleon momentum distribution



Hui Xue<sup>a</sup>, Chang Xu<sup>a,\*</sup>, Gao-Chan Yong<sup>b</sup>, Zhongzhou Ren<sup>a</sup>

<sup>a</sup> Department of Physics and Key Laboratory of Modern Acoustics, Nanjing University, Nanjing 210008, China

<sup>b</sup> Institute of Modern Physics, Chinese Academy of Sciences, Lanzhou 730000, China

## ARTICLE INFO

### Article history:

Received 14 October 2015

Received in revised form 24 January 2016

Accepted 22 February 2016

Available online 26 February 2016

Editor: W. Haxton

### Keywords:

Neutron–proton bremsstrahlung

High-momentum component

Nucleus–nucleus collision

## ABSTRACT

Neutron–proton bremsstrahlung in intermediate energy nucleus–nucleus collisions is proposed as a possible probe to study the high-momentum component in nucleon momentum distribution of finite nucleus. Based on the Boltzmann–Uehling–Uhlenbeck (BUU) transport model, the effects of high-momentum component on the production of bremsstrahlung photons in the reaction of  $^{12}\text{C} + ^{12}\text{C}$  collisions at different incident beam energies are studied. It is found that the high-momentum component increases the high-energy bremsstrahlung photon production remarkably. Furthermore, the ratio of photon production at different incident beam energies is suggested as a potential observable to probe the high-momentum component in nucleon momentum distribution of finite nucleus.

© 2016 The Authors. Published by Elsevier B.V. This is an open access article under the CC BY license (<http://creativecommons.org/licenses/by/4.0/>). Funded by SCOAP<sup>3</sup>.

## 1. Introduction

The nucleon momentum distribution  $n(k)$  is a quantity of particular interest for both finite nuclei and nuclear matter [1]. It contains information of the mean-field properties as well as the short-range behavior of the nucleon–nucleon correlations [1]. In the past several years, the nucleon momentum distributions in both symmetric and asymmetric nuclear systems have attracted much attention from both theoretical and experimental sides. Theoretical investigations have shown that the short-range-correlated (SRC) pairs induced by tensor force can push nucleons from low momenta to high momenta, creating a high-momentum tail (HMT) in the nucleon momentum distribution [1]. This was also investigated by the high energy electron scattering experiment conducted by the Jefferson Lab (JLab) using finite nucleus  $^{12}\text{C}$  [2]. The experimental results of the JLab suggest that about 20% of nucleons are correlated in  $^{12}\text{C}$  and 90% of the correlated pairs are in the form of  $np$  SRC pairs [2]. The dominance of the  $np$  over  $pp$  SRC pairs is a consequence of the existence of tensor force in the  $np$  deuteron-like state [3,4]. More recently, the high energy electron scattering measurements in the JLab further show that even in heavy, neutron-rich nuclei (such as  $^{27}\text{Al}$ ,  $^{56}\text{Fe}$ , and  $^{208}\text{Pb}$ ), the short-range interactions between the nucleons can form correlated high-momentum pairs [5]. Both the SRC and the high-momentum

component in nucleon momentum distribution are closely related to a number of issues in nuclear structure and reaction [6–14]. For instance, the tensor force induced SRC is found to be particularly important to determine the nuclear symmetry energy and its high density behavior [8,9]. It is shown that the high-momentum component in nucleon momentum distribution can result in much larger average kinetic energies of nucleons in symmetric nuclear matter as compared to the free Fermi gas (FFG) predictions [11, 13]. The kinetic part of symmetry energy thus turns out to be very small (even negative) by taking into account the high-momentum component in nucleon momentum distribution [11]. This interesting feature is further confirmed by the more sophisticated Bruckner Hartree–Fock and self-consistent Green function calculations [12,14,15].

The purpose of this work is to investigate the possibility to probe nucleon high-momentum component by using the neutron–proton bremsstrahlung photons in nucleus–nucleus collisions. Due to the near absence of the meson exchange contribution and the relatively weak multipole radiation, the intensity of proton–proton bremsstrahlung is usually one order of magnitude smaller than that of proton–neutron bremsstrahlung [16,17]. Therefore we do not consider the proton–proton bremsstrahlung in the present work. The merit of photons is that they interact with nucleons only electromagnetically. The neutron–proton bremsstrahlung in the early stage of the reaction is found to be the main source of the photon production [18,19]. Once the photons are produced in collisions, they escape almost freely from the nuclear environment in nuclear reactions. This makes photon production to be a clean

\* Corresponding author.

E-mail address: [cxu@nju.edu.cn](mailto:cxu@nju.edu.cn) (C. Xu).

probe in nucleus–nucleus collisions. The bremsstrahlung photons were successfully used to study a number of properties such as the nuclear caloric curve, the dynamics of nucleon–nucleon interactions, and the time-evolution of the reaction process before nuclear break-up [20–23]. For intermediate energy nucleus–nucleus collisions, the high-momentum component in nucleon momentum distribution increases the average nucleon kinetic energies of both projectile and target, and thus it is expected to increase the high-energy photon production from bremsstrahlung as well. This may provide a possible way to investigate the nucleon momentum distribution in finite nucleus by measuring the high-energy bremsstrahlung photons produced in intermediate energy collisions. In this study, we use the isospin dependent Boltzmann–Uehling–Uhlenbeck (BUU) transport model [24–26] to simulate collisions of two  $^{12}\text{C}$  nuclei at different incident energies. We compare the photon production in the  $^{12}\text{C} + ^{12}\text{C}$  collisions by assuming two kinds of momentum distribution for  $^{12}\text{C}$ : 1) momentum distribution of free Fermi gas (FFG); 2) momentum distribution with a high-momentum tail (HMT) based on Refs. [5,6]. Investigations have suggested that the HMT in single-nucleon momentum distribution is very similar for nuclei from deuteron to infinite nuclear matter [27–31], roughly exhibits a  $C/k^4$  tail where  $k$  is the nucleon momentum and  $C$  is a parameter [5,6,32–34]. We choose the HMT with the form of  $C/k^4$  in our present simulations according to Refs. [5,6,32–34]. By comparing the results using two different kinds of momentum distributions, we find that neutron–proton bremsstrahlung and the corresponding high-energy photon production are sensitive to the HMT in nucleon momentum distribution.

The double differential probabilities of photon production with different kinds of mean-field potentials and different incident beam energies are given in details. And the ratio of the double differential photon production probabilities at different incident beam energies is suggested as a possible probe for the nucleon momentum distribution in finite nucleus. This paper is organized as follows: In section 2, the theoretical framework of BUU model and the photon production formula is briefly reviewed. The numerical results and discussions are presented in section 3. Finally, section 4 concludes the paper.

## 2. Brief review of theoretical framework of BUU model and photon production

Our present simulations of intermediate energy  $^{12}\text{C} + ^{12}\text{C}$  collisions are based on the isospin-dependent Boltzmann–Uehling–Uhlenbeck (BUU) transport model [24–26]. The BUU transport model is quite successful in describing dynamical evolution of nucleus–nucleus collisions and the main equation of the BUU model is given by:

$$\frac{\partial f}{\partial t} + \vec{v} \cdot \nabla_r f - \nabla_r U \cdot \nabla_p f = I_{\text{collision}}, \quad (1)$$

where  $f(\vec{r}, \vec{p}, t)$  is the probability of finding a particle at time  $t$  with momentum  $\vec{p}$  at position  $\vec{r}$ . The function  $f$  can be considered as a mathematical tool facilitating quantum calculations as long as it yields a reasonable description of final observables after collisions [35,36]. The quantum physics plays a role in the initial condition on  $f$ , which must respect the Pauli principle. The mean-field potential  $U$  is an important input for BUU model. The left-hand side of Eq. (1) denotes the time evolution of the particle phase space distribution function due to its transport and mean field, and the collision term  $I_{\text{collision}}$  on the right-hand side governs the modifications of  $f(\vec{r}, \vec{p}, t)$  by elastic and inelastic two body collisions caused by short-range residual interactions.

$$I_{\text{collision}} = -\frac{1}{(2\pi)^3} \int d^3 p_2 d^3 p_2' d\Omega \frac{d\sigma}{d\Omega} v_{12} \times \delta^3(\vec{p} + \vec{p}_2 - \vec{p}'_1 - \vec{p}'_2) \times [ff_2(1-f_1')(1-f_2') - f_1'f_2'(1-f)(1-f_2)], \quad (2)$$

where  $\frac{d\sigma}{d\Omega}$  is the in-medium NN cross section.  $v_{12}$  is the relative velocity for the two colliding nucleons 1 and 2. When the nucleons 1 and 2 collide they change from  $(\vec{r}_1, \vec{p}_1)(\vec{r}_2, \vec{p}_2)$  to  $(\vec{r}_1, \vec{p}_1')(\vec{r}_2, \vec{p}_2')$ . Considering the Pauli blocking effect, such scattering is allowed if the phase-spaces around  $(\vec{r}_1, \vec{p}_1')$  and  $(\vec{r}_2, \vec{p}_2')$  are essentially empty. If they are filled, the scattering should be suppressed. The Pauli blocking effect is embodied in terms  $(1-f_1')(1-f_2')$  and  $(1-f_1)(1-f_2)$  in Eq. (2).

Two different kinds of mean-field potentials  $U$  are implemented in our calculations for comparison [37,38]. One is the momentum-dependent potential deduced from the Gogny effective interaction (MDI) [37]:

$$U(\rho, \delta, \vec{p}, \tau) = A_u(x) \frac{\rho_{\tau'}}{\rho_0} + A_l(x) \frac{\rho_{\tau}}{\rho_0} + B \left( \frac{\rho}{\rho_0} \right)^{\sigma} (1 - x\delta^2) - 8x\tau \frac{B}{\sigma + 1} \frac{\rho^{\sigma-1}}{\rho_0^{\sigma}} \delta \rho_{\tau'} + \frac{2C_{\tau, \tau}}{\rho_0} \int d^3 \vec{p}' \frac{f_{\tau}(\vec{r}, \vec{p}')}{1 + (\vec{p} - \vec{p}')^2 / \Lambda^2} + \frac{2C_{\tau, \tau'}}{\rho_0} \int d^3 \vec{p}' \frac{f_{\tau'}(\vec{r}, \vec{p}')}{1 + (\vec{p} - \vec{p}')^2 / \Lambda^2}, \quad (3)$$

where  $\tau(\tau') = 1/2(-1/2)$  for neutron (proton),  $\rho_n(\rho_p)$  denotes neutron (proton) density,  $\rho = \rho_n + \rho_p$  is the nucleon density,  $\delta = (\rho_n - \rho_p)/(\rho_n + \rho_p)$  is the isospin asymmetry and the values of the parameters  $A_u(x)$ ,  $A_l(x)$ ,  $B$ ,  $C_{\tau, \tau}$ ,  $C_{\tau, \tau'}$ ,  $\sigma$ , and  $\Lambda$  can be found in Ref. [37]. The choice of parameter  $x$  has negligible effect on the final results of  $^{12}\text{C} + ^{12}\text{C}$  collisions as  $^{12}\text{C}$  is a symmetric nuclear system. The other is the momentum-independent soft Bertsch–Kruse–Das Gupta (SBKD) potential [38]:

$$U(\rho) = A(\rho/\rho_0) + B(\rho/\rho_0)^{\sigma}, \quad (4)$$

where  $\rho$  is the nucleon density and  $\rho_0 = 0.16 \text{ fm}^{-3}$  is the saturation density. The values of three parameters are  $A = -356 \text{ MeV}$ ,  $B = 303 \text{ MeV}$ , and  $\sigma = 7/6$  [38]. Besides the choice of mean-field potential, the value of nucleon–nucleon elastic cross section is also an important input in the BUU model. Here the isospin-dependent in-medium nucleon–nucleon cross section using nucleon effective mass is given by:

$$\sigma_{NN}^{\text{medium}} = \sigma_{NN}^{\text{free}} \cdot (\mu_{NN}^* / \mu_{NN})^2, \quad (5)$$

where  $\mu_{NN}$  and  $\mu_{NN}^*$  are the free-space reduced mass and in-medium reduced mass of the colliding nucleon pair, respectively.  $\sigma_{NN}^{\text{free}}$  is the free-space nucleon–nucleon cross section taken from experimental data [39]. In the BUU simulations, the effect of the nuclear equation of state (EOS) could be important for many final observables. However, it is already found in previous studies that its effect on the photon production is small [40].

Usually the bremsstrahlung photon production probability in intermediate energy reactions is very small, roughly a thousand nucleon–nucleon collisions produce a photon. The influence induced by bremsstrahlung on the kinematics of nucleons is very small, thus a perturbative approach could be used to calculate the photon production probability. Specifically, the photon production can be calculated as a probability at each neutron–proton collision and the total photon production probability is obtained by

summing over all neutron–proton collisions over the entire history of the reaction. The elementary probability for neutron–proton bremsstrahlung can be obtained by using the semiclassical hard sphere collision model [41] and other methods involving more quantum-mechanical effects such as the one boson exchange (OBE) model [42–47]. Based on the OBE model, a good fitting expression of the double differential photon production probability is given by Gan et al. [47]:

$$\frac{d^2 P}{d\Omega dE_\gamma} = 1.6 \times 10^{-7} \frac{(1-y^2)^\alpha}{y}, \quad (6)$$

where the ratio  $y = E_\gamma/E_{max}$ .  $E_\gamma$  is the energy of the produced photon and  $E_{max}$  is the energy available in the proton–neutron center of momentum frame, i.e.,  $E_{max} = 2 \times (m - m_0)$ .  $m_0$  is the rest mass of proton and  $m$  is the relativistic mass of proton. The parameter  $\alpha$  is fitted to be  $\alpha = 0.7319 - 0.5898\beta_i$  with  $\beta_i = p/m$  and  $p$  is the momentum of the proton. This expression of double differential photon production probability has been successfully used in Refs. [39,47,48] and reproduces the experimental data reasonably [47].

### 3. Parameterization of momentum distribution and numerical results of BUU simulations

In the BUU simulation, before the reaction starts, an initialization is made to obtain the initial phase-space function  $f(\vec{r}, \vec{p}, t = 0)$ . The initial  $f$  is dependent on the nucleon momentum distributions in both target and projectile nuclei. Thus, the nucleon momentum distribution enters in the BUU formalism through the function  $f$ . For symmetric nuclear systems, we assume that protons and neutrons have the same momentum distribution. In this work, two different initial single-nucleon momentum distributions in symmetric nuclear matter (SNM) are used for BUU simulations. The first one is the uncorrelated free Fermi gas (FFG) distribution that exhibits a step function, i.e., a constant for  $k \leq k_F$ , and zero for  $k > k_F$  where  $k_F$  is the Fermi momentum. The second one is the single-nucleon momentum distribution with a high-momentum tail (HMT). As shown in Fig. 1, the solid line step function stands for  $n(k)$  of FFG, and the dashed line corresponds to  $n(k)$  with SRC induced HMT. The latter is given according to Ref. [6] as follows:

$$n_{SNM}(k) = \begin{cases} C_1 & (k \leq k_F) \\ C_2/k^4 & (k_F < k \leq \lambda k_F), \\ 0 & (k > \lambda k_F) \end{cases}, \quad (7)$$

where the Fermi momentum  $k_F$  is  $[3\pi^2 \rho_{p(n)}]^{1/3}$ . The  $\lambda \approx 2.75$  is the high-momentum cutoff [6,32]. The parameters  $C_1$  and  $C_2$  are determined by the normalization condition:

$$4\pi \int_0^\infty n_{SNM}(k) k^2 dk = 1, \quad (8)$$

and the condition that roughly 25% nucleons are involved in the HMT [6]:

$$4\pi \int_{k_F}^\infty n_{SNM}(k) k^2 dk = 0.25. \quad (9)$$

Based on the local-density approximation [47,49], the nucleon momentum distribution in finite nucleus such as  $^{12}\text{C}$  can be easily obtained from that in symmetric nuclear matter. The nucleon momentum distribution in finite nucleus is given by [47,49]:

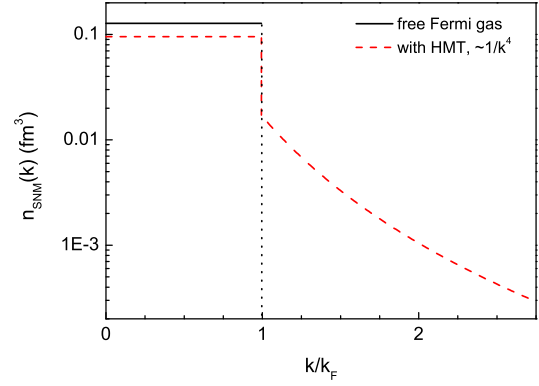


Fig. 1. The single-nucleon momentum distribution in symmetric nuclear matter. The solid line stands for the uncorrelated FFG case, while the dashed line stands for the correlated case, which has a  $\sim 1/k^4$  HMT.

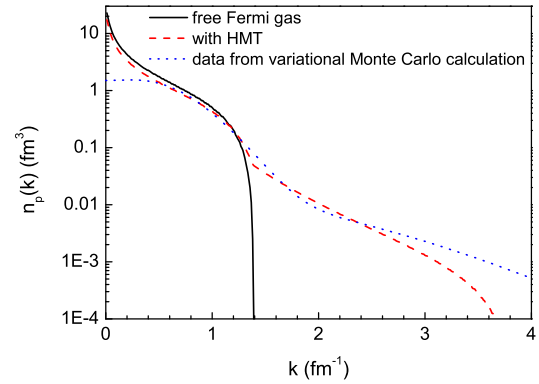
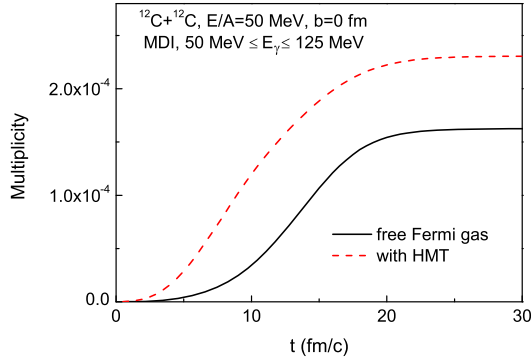


Fig. 2. The proton momentum distribution in  $^{12}\text{C}$  deduced from the local-density approximation. The solid line denotes the FFG case while the dashed line is the HMT case. The dotted line is the proton momentum distribution taken from the state-of-the-art variational Monte Carlo calculation [50].

$$n_{p(n)}(k) = \int d^3r \rho_{p(n)}(r) n_{SNM}(k, k_F(r)), \quad (10)$$

where  $n_{p(n)}(k)$  is the proton (neutron) momentum distribution in finite nucleus  $^{12}\text{C}$ .  $n_{SNM}(k, k_F(r))$  is the single-nucleon momentum distribution in symmetric nuclear matter. The Fermi momentum  $k_F(r)$  is  $[3\pi^2 \rho_{p(n)}(r)]^{1/3}$  and  $\rho_{p(n)}(r)$  is the proton (neutron) density distribution in  $^{12}\text{C}$ . Fig. 2 shows the calculated proton momentum distribution in  $^{12}\text{C}$  where the solid and dashed lines stand for the FFG and HMT cases, respectively. The dotted line is the proton momentum distribution taken from the state-of-the-art variational Monte Carlo calculation [50]. Although we use an analytical parameterization to obtain the nucleon momentum distribution in  $^{12}\text{C}$ , it can be seen from Fig. 2 that our calculated  $n_p(k)$  with HMT can reasonably fit the proton momentum distribution taken from the state-of-the-art calculation in the important region from  $0.5 \text{ fm}^{-1}$  to  $2.5 \text{ fm}^{-1}$  [50]. The neutron momentum distribution in  $^{12}\text{C}$  can be given using the same method and thus we do not repeat it.

With two different kinds of nucleon momentum distributions in  $^{12}\text{C}$ , we firstly carry out the numerical simulations of  $^{12}\text{C} + ^{12}\text{C}$  collisions using the MDI mean-field potential at a beam energy of 50 MeV/nucleon. We will focus on the bremsstrahlung photons produced in the  $^{12}\text{C} + ^{12}\text{C}$  collisions, especially the high-energy bremsstrahlung photons ( $E_\gamma \geq 50 \text{ MeV}$ ). Fig. 3 shows the time evolution of the multiplicity of bremsstrahlung photons with energy  $50 \text{ MeV} \leq E_\gamma \leq 125 \text{ MeV}$  in the head-on collisions, where the solid and dashed lines stand for simulation results of the FFG and HMT cases, respectively. It can be clearly seen that the HMT leads to an obvious increase of high-energy photons ( $50 \text{ MeV} \leq E_\gamma \leq$



**Fig. 3.** Time evolution of the multiplicity of high-energy photons with  $50 \text{ MeV} \leq E_\gamma \leq 125 \text{ MeV}$  in  $^{12}\text{C} + ^{12}\text{C}$  head-on collisions at the beam energy of  $50 \text{ MeV/nucleon}$ , in the FFG and HMT cases.

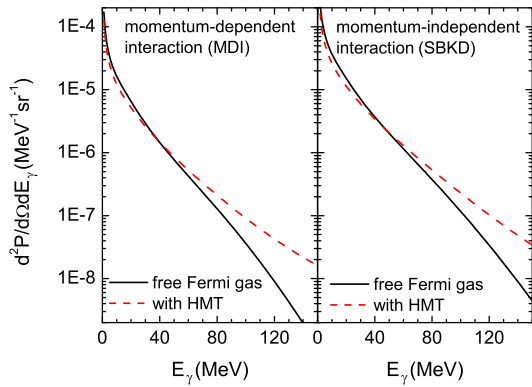


**Fig. 4.** The double differential probabilities of photon production in  $^{12}\text{C} + ^{12}\text{C}$  head-on collisions at the beam energy of  $50 \text{ MeV/nucleon}$  using momentum-dependent interaction (MDI) and momentum-independent interaction (SBKD), respectively.

$125 \text{ MeV}$ ) from bremsstrahlung. This is not surprising as the HMT increases the average nucleon kinetic energy in both the projectile and target, and thus the yield of high-energy bremsstrahlung photons is increased as well.

It is noted the results in Fig. 3 are obtained by using the MDI mean-field potential in BUU simulations. To test the effect of different mean-field potentials on the photon production in  $^{12}\text{C} + ^{12}\text{C}$  collisions, we further compare the results from the above momentum-dependent MDI interaction [37] with another momentum-independent interaction, namely the SBKD interaction [38]. Fig. 4 gives the double differential probabilities of photon production using MDI and SBKD interactions, respectively. It is clearly seen that in both cases HMT results in an obvious increase of high-energy photon production and a decrease of low-energy photon production. It is also seen from Fig. 4 that the effect of different mean-field potentials on photon production is relatively small as compared with the HMT effect.

We also investigate the photon production in  $^{12}\text{C} + ^{12}\text{C}$  head-on collisions at different incident beam energies. Fig. 5 compares the double differential probabilities of photon production using MDI interaction at incident beam energies of  $50 \text{ MeV/nucleon}$  and  $140 \text{ MeV/nucleon}$ , respectively. It is clearly shown in Fig. 5 that, for both energies, the HMT in nucleon momentum distribution has the same effect on the high energy photon production. For instance, at  $E_{beam} = 50 \text{ MeV/nucleon}$ , the multiplicity of high-energy photons ( $50 \text{ MeV} < E_\gamma < 125 \text{ MeV}$ ) is  $1.65 \times 10^{-4}$  in the FFG case, but increases to  $2.31 \times 10^{-4}$  in the HMT case. This corresponds to a 40% growth of the photon production. At  $E_{beam} = 140 \text{ MeV/nucleon}$ , the multiplicity of corresponding high-energy photons ( $140 \text{ MeV} <$

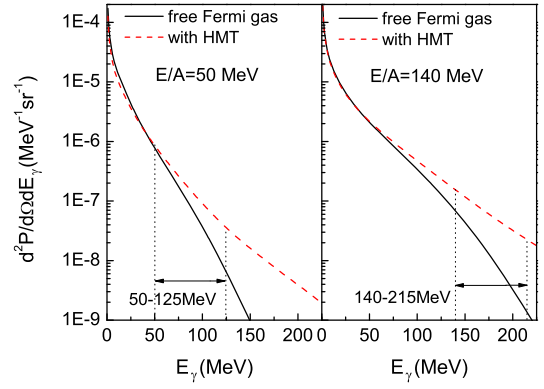


**Fig. 5.** The effects of the HMT on the double differential probability of photon production in  $^{12}\text{C} + ^{12}\text{C}$  head-on collisions at beam energy of  $50 \text{ MeV/nucleon}$  and  $140 \text{ MeV/nucleon}$ .

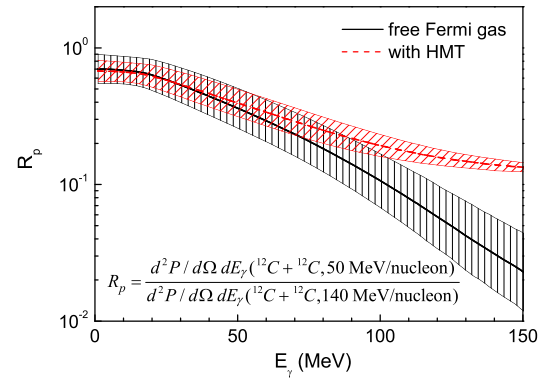


**Fig. 6.** Ratio of double differential photon production probabilities at incident beam energies of  $50 \text{ MeV/nucleon}$  and  $140 \text{ MeV/nucleon}$  in  $^{12}\text{C} + ^{12}\text{C}$  head-on collision. The bands represent the uncertainties of the calculations.

$E_\gamma < 215 \text{ MeV}$ ) is  $1.8 \times 10^{-5}$  in the FFG case while  $6.4 \times 10^{-5}$  in the HMT case.

We have shown the effects of different mean-field potentials and different beam energies on the photon production from bremsstrahlung. However, there are some other factors which may affect the photon production, such as the nucleon–nucleon scattering cross section, the stability of initial colliding nuclei, and the uncertainty in photon production probability, etc. To reduce the effects of these unresolved factors, the ratio of some observables from double reaction system is possibly a way out in the present BUU model [39,48]. Here we use the ratio of double differential photon production  $R_p$  at two different incident beam energies  $50 \text{ MeV/nucleon}$  and  $140 \text{ MeV/nucleon}$ ,

$$R_p = \frac{d^2P/d\Omega dE_\gamma(^{12}\text{C} + ^{12}\text{C}, 50 \text{ MeV/nucleon})}{d^2P/d\Omega dE_\gamma(^{12}\text{C} + ^{12}\text{C}, 140 \text{ MeV/nucleon})}. \quad (11)$$

The ratio  $R_p$  as a function of photon energy  $E_\gamma$  with the error bar is plotted in Fig. 6. It can be seen that the value of  $R_p$  is less than 1 for all photon energy range ( $0-150 \text{ MeV}$ ). It is because that higher incident beam energy  $E_{beam} = 140 \text{ MeV/nucleon}$  leads to larger photon yield as compared with the photon yield at  $E_{beam} = 50 \text{ MeV/nucleon}$ . It is also seen from Fig. 6 that  $R_p$  is sensitive to the HMT effect by comparing with the FFG case in high photon energy range ( $E_\gamma > 100 \text{ MeV}$ ). In Fig. 6, we also give the error bar of the ratio  $R_p$ . The error bar is large in the case of FFG for all energy range. Surprisingly, the error bar of  $R_p$  in the HMT case becomes much smaller with the increasing of energy  $E_\gamma$ . This is possibly due to that the higher energy photons

are mainly produced from the collisions of HMT nucleons and the uncertainties from NN cross section and photon production probability are largely reduced. More importantly, there is no crossover between FFG and HMT cases with  $E_\gamma > 100$  MeV. This is helpful to distinguish these two cases in experiments. Thus ratio  $R_p$  could be a good probe to study the HMT in nucleon momentum distribution of finite nucleus. The SRC induced HMT, in principle, should be included self-consistently in the nucleus–nucleus collision simulations. However, this is very difficult within the frame work of present BUU model, and some factors such as the nucleon off-shell effect can not be fully taken into account [20]. Thus the further development of transport model will be helpful to pin down the SRC induced HMT through nucleus–nucleus collisions, which is of great importance in studying the nuclear symmetry energy and the physics of neutron stars.

#### 4. Summary

In summary, in the framework of the BUU transport model, we have carried out a study of the effect of nucleon momentum distribution on the bremsstrahlung photon production in the reaction of  $^{12}\text{C} + ^{12}\text{C}$  collision. It is found that the neutron–proton bremsstrahlung photons are sensitive to the high-momentum component in nucleon momentum distribution of  $^{12}\text{C}$ . We also investigated the effect of different mean-field potentials and different incident beam energies on the photon production. Double differential probabilities of photon production are discussed in details. Canceling out uncertainties from mean-field potential and  $np$  scattering cross section as well as from photon production probability, etc., the ratio of photon production at different incident beam energies is proposed to probe the high-momentum component in nucleon momentum distribution of finite nucleus.

#### Acknowledgements

This work is supported by the National Natural Science Foundation of China (Grants No. 11175085, No. 11575082, No. 11235001, No. 11535004, No. 11375086, No. 11375239 and No. 11120101005), by the 973 Program of China (Grant No. 2013CB834400), and by the Project Funded by the Priority Academic Program Development of Jiangsu Higher Education Institutions (PAPD).

#### References

- [1] A.N. Antonov, P.E. Hodgson, I.Z. Petkov, *Nucleon Momentum and Density Distributions in Nuclei*, Clarendon Press, Oxford, 1988.
- [2] R. Subedi, et al., *Science* 320 (2008) 1476.
- [3] M.M. Sargsian, T.V. Abrahamyan, M.I. Strikman, L.L. Frankfurt, *Phys. Rev. C* 71 (2005) 044615.
- [4] R. Schiavilla, R.B. Wiringa, S.C. Pieper, J. Carlson, *Phys. Rev. Lett.* 98 (2007) 132501.
- [5] O. Hen, et al., *Science* 346 (2014) 614.
- [6] O. Hen, B.A. Li, W.J. Guo, L.B. Weinstein, E. Piasetzky, *Phys. Rev. C* 91 (2015) 025803.
- [7] B.A. Li, L.W. Chen, C.M. Ko, *Phys. Rep.* 464 (2008) 113.
- [8] C. Xu, B.A. Li, *Phys. Rev. C* 81 (2010) 044603.
- [9] C. Xu, B.A. Li, *Phys. Rev. C* 81 (2010) 064612.
- [10] C. Xu, B.A. Li, L.W. Chen, *Phys. Rev. C* 82 (2010) 054607.
- [11] C. Xu, A. Li, B.A. Li, J. Phys. Conf. Ser. 420 (2013) 012090.
- [12] I. Vidaña, A. Polls, C. Providência, *Phys. Rev. C* 84 (2011) 062801(R).
- [13] X. Zhang, C. Xu, Z.Z. Ren, *Eur. Phys. J. A* 50 (2014) 113.
- [14] A. Rios, A. Polls, W.H. Dickhoff, *Phys. Rev. C* 89 (2014) 044303.
- [15] A. Carbone, A. Polls, A. Rios, *Europhys. Lett.* 97 (2012) 22001.
- [16] V. Herrmann, J. Speth, K. Nakayama, *Phys. Rev. C* 43 (1991) 394.
- [17] Y. Saffkan, et al., *Phys. Rev. C* 75 (2007) 031001(R).
- [18] G.H. Liu, Y.G. Ma, X.Z. Cai, D.Q. Fang, W.Q. Shen, W.D. Tian, K. Wang, *Phys. Lett. B* 663 (2008) 312.
- [19] Y.G. Ma, G.H. Liu, X.Z. Cai, D.Q. Fang, W. Guo, W.Q. Shen, W.D. Tian, H.W. Wang, *Phys. Rev. C* 85 (2012) 024618.
- [20] Y. Schutz, et al., *Nucl. Phys. A* 622 (1997) 404.
- [21] G. Martinez, et al., *Phys. Lett. B* 461 (1999) 28.
- [22] D. d'Enterria, et al., *Phys. Lett. B* 538 (2002) 27.
- [23] R. Ortega, et al., *Eur. Phys. J. A* 28 (2006) 161.
- [24] B.A. Li, Z.Z. Ren, C.M. Ko, S.J. Yennello, *Phys. Rev. Lett.* 76 (1996) 4492.
- [25] B.A. Li, C.M. Ko, Z.Z. Ren, *Phys. Rev. Lett.* 78 (1997) 1644.
- [26] B.A. Li, C.B. Das, S. Das Gupta, C. Gale, *Nucl. Phys. A* 735 (2004) 563.
- [27] C. Giori degli Atti, S. Simula, *Phys. Rev. C* 53 (1996) 1689.
- [28] S.C. Pieper, R.B. Wiringa, V.R. Pandharipande, *Phys. Rev. C* 46 (1992) 1741.
- [29] K.Sh. Egiyan, et al., *Phys. Rev. C* 68 (2003) 014313.
- [30] L. Frankfurt, M. Sargsian, M. Strikman, *Int. J. Mod. Phys. A* 23 (2008) 2991.
- [31] J. Arrington, D.W. Higinbotham, G. Rosner, M. Sargsian, *Prog. Part. Nucl. Phys.* 67 (2012) 898.
- [32] O. Hen, L.B. Weinstein, E. Piasetzky, G.A. Miller, M.M. Sargsian, Y. Sagi, arXiv:1407.8175v3, 2015.
- [33] B.J. Cai, B.A. Li, *Phys. Rev. C* 92 (2015) 011601(R).
- [34] R. Weiss, B. Bazak, N. Barnea, *Phys. Rev. Lett.* 114 (2015) 012501.
- [35] G.F. Bertsch, S. Das Gupta, *Phys. Rep.* 160 (1988) 189.
- [36] H.W. Lee, *Phys. Rep.* 259 (1995) 147.
- [37] C.B. Das, S. Das Gupta, C. Gale, B.A. Li, *Phys. Rev. C* 67 (2003) 034611.
- [38] G.F. Bertsch, H. Kruse, S. Das Gupta, *Phys. Rev. C* 29 (1984) 673.
- [39] G.C. Yong, W. Zuo, X.C. Zhang, *Phys. Lett. B* 705 (2011) 240.
- [40] C.M. Ko, J. Aichelin, *Phys. Rev. C* 35 (1987) 1976.
- [41] J.D. Jackson, *Classical Electrodynamics*, Wiley, New York, 1962, Chapter 14.
- [42] H. Nifenecker, J.P. Bondorf, *Nucl. Phys. A* 442 (1985) 478.
- [43] K. Nakayama, G.F. Bertsch, *Phys. Rev. C* 34 (1986) 2190.
- [44] K. Nakayama, *Phys. Rev. C* 39 (1989) 1475.
- [45] V. Herrmann, J. Speth, K. Nakayama, *Phys. Rev. C* 43 (1991) 394.
- [46] M. Schäffer, T.S. Biro, W. Cassing, U. Mosel, H. Nifenecker, J.A. Pinstan, *Z. Phys. A* 339 (1991) 391.
- [47] N. Gan, et al., *Phys. Rev. C* 49 (1994) 298.
- [48] G.C. Yong, B.A. Li, L.W. Chen, *Phys. Lett. B* 661 (2008) 82.
- [49] L. Viverit, S. Giorgini, L.P. Pitaevskii, S. Stringari, *Phys. Rev. A* 69 (2004) 013607.
- [50] R.B. Wiringa, R. Schiavilla, S.C. Pieper, J. Carlson, *Phys. Rev. C* 89 (2014) 024305.